Schmidt modes in the angular spectrum of bright squeezed vacuum

P. Sharapova,[1] A. M. Pérez,[2,3] O. V. Tikhonova,[1,4] and M. V. Chekhova[1,2,3]

[1]*Physics Department, Moscow State University, Leninskiye Gory 1-2, Moscow 119991, Russia*

[2]*Max-Planck Institute for the Science of Light, Guenther-Scharowsky-Str. 1/Bau 24, Erlangen D-91058, Germany*

[3]*University of Erlangen-Nürnberg, Staudtstrasse 7/B2, 91058 Erlangen, Germany*

[4]*Skobeltsyn Institute of Nuclear Physics, Lomonosov Moscow State University, Moscow 119234, Russia*

(Received 24 October 2014; revised manuscript received 13 January 2015; published 10 April 2015)

We investigate both theoretically and experimentally strong correlations in macroscopic (bright) quantum states of light generated via unseeded parametric down-conversion and four-wave mixing. The states generated this way contain only quantum noise, without a classical component, and are referred to as bright squeezed vacuum (BSV). Their important advantage is the multimode structure, which offers a larger capacity for the encoding of quantum information. For the theoretical description of these states and their correlation features we introduce a generalized fully analytical approach, based on the concept of independent collective (Schmidt) modes and valid for the cases of both weak and strong nonlinear interaction. In experiment, we generate states of macroscopic BSV with up to 10^{10} photons per mode and examine large photon-number spatial correlations that are found to be very well described by our theoretical approach.

DOI: 10.1103/PhysRevA.91.043816 PACS number(s): 42.50.Dv, 42.50.Lc, 42.65.Lm, 42.65.Yj

I. INTRODUCTION

Currently, much interest is attracted to bright squeezed vacuum (BSV), a macroscopic nonclassical state of light that can be obtained via high-gain parametric down-conversion (PDC) or four-wave mixing (FWM). This is because BSV contains huge photon numbers and at the same time is strongly nonclassical, consisting of only quantum noise, without a classical component, and manifesting entanglement [1] and noise reduction below the standard quantum limit [2]. These features make it interesting for applications such as quantum imaging [3,4] and metrology [5,6], quantum optomechanics [7], and nonlinear optics with quantum light [8]. In addition, large photon-number correlations arising in BSV are richer than entanglement in two-photon light emitted via low-gain PDC or FWM [9]. An important advantage of such states is their multimode structure, which offers a larger capacity for the encoding of quantum information.

In contrast to low-gain PDC or FWM, developing a consistent theoretical description of their high-gain analogs is a difficult problem due to the contribution of correlated high-order Fock components and, therefore, nonapplicability of the perturbation theory. Several recent theoretical investigations of such high-gain regimes are based on the concept of collective input/output modes introduced mostly to describe the spectral properties in the frequency domain [10–15] and followed by the Bloch-Messiah reduction [16]. However, beyond the perturbation approach the solution for the field operators was up to now obtained only numerically, usually through a set of integrodifferential equations [13,14,17–19], which does not clarify the mechanisms of the observed effects.

Here we present a fully analytical description of the angular properties of PDC and FWM, valid both for weak and strong nonlinear interaction. Our approach is based on the Bloch-Messiah reduction and allows one to obtain the evolution of the photon creation (annihilation) operators both for the Schmidt modes and for the commonly used plane-wave modes as well as to calculate various correlation characteristics of BSV. It should be emphasized that the applied formalism allows one to find the effective number of independent collective modes of the system, a measure of its information capacity. Meanwhile, we generate BSV via high-gain PDC and perform a series of experiments on its spatial spectrum and correlations. The measurement results are in a very good agreement with our analytical predictions. The developed theoretical approach is rather general, can be applied to different bipartite quantum systems, and sheds light on the physical nature of strong multiphoton correlations of BSV states that can be understood in terms of independent collective modes. Further we consider several interesting effects observed experimentally, such as photon-number correlations in the angular spectrum, their dependence on the parametric gain, and the manifestation of the transverse walkoff, and explain them using the developed theoretical approach.

The paper is organized as follows. Section II describes our theoretical approach, based on the Bloch-Messiah reduction and leading to the theoretical expressions for the observable quantities. Section III presents an experiment on the measurement of the angular spectrum and correlations in the PDC radiation. In Sec. IV, the dependence of the spectrum on the parametric gain is studied and compared to the results known from the literature. An experiment on the observation of anisotropy effects in high-gain PDC radiation is described in Sec. V. Conclusions are given in Sec. VI, and the four Appendices are devoted to the theoretical description of the two-crystal scheme (Appendix A), deriving explicit expressions for the plane-wave observables (Appendix B), the use of the Cartesian frame of reference and the double-Gauss model (Appendix C), and the case of strong anisotropy (Appendix D).

II. BLOCH-MESSIAH REDUCTION

At any parametric gain, PDC is described by the Hamiltonian of the form

$$H \sim \int d^3\mathbf{r}\chi^{(2)}(\mathbf{r})E_p^{(+)}(\mathbf{r},t)E_s^{(-)}(\mathbf{r},t)E_i^{(-)}(\mathbf{r},t) + \text{H.c.},$$

where $\chi^{(2)}(\mathbf{r})$ is the quadratic nonlinearity and s,i,p indices correspond to the signal, idler, and pump radiation, respectively. A similar description, with $\chi^{(2)}$ replaced by the cubic nonlinearity and $E_p^{(+)}$ entering twice, is valid for FWM [20]. After integrating over space, assuming that the pump amplitude has a Gaussian spatial distribution, we obtain the Hamiltonian in the simplest case of type-I PDC in one nonanisotropic nonlinear crystal:

$$H = i\hbar\Gamma \int d\mathbf{q}_s d\mathbf{q}_i F(\mathbf{q}_s,\mathbf{q}_i) a^\dagger_{\mathbf{q}_s} a^\dagger_{\mathbf{q}_i} + \text{H.c.}, \tag{1}$$

with the two-photon amplitude (TPA)

$$F(\mathbf{q}_s,\mathbf{q}_i) = C \exp\left\{-\frac{\sigma^2(\mathbf{q}_s+\mathbf{q}_i)^2}{2}\right\} \text{sinc}\left(\frac{L(\mathbf{q}_s-\mathbf{q}_i)^2}{4k_p}\right) \times \exp\left\{i\frac{L(\mathbf{q}_s-\mathbf{q}_i)^2}{4k_p}\right\}, \tag{2}$$

where Γ is the coupling parameter, $\mathbf{q}_{s,i}$ the transverse components of the signal and idler wave vectors, $a^\dagger_{\mathbf{q}_{s,i}}$ the photon creation operators for the corresponding plane-wave modes, C the normalization constant, $2\sqrt{\ln 2}\sigma$ the full width at half maximum (FWHM) of the pump spatial intensity distribution, L the crystal length, and k_p the pump wave vector.

For simplicity we assume that $\omega_s = \omega_i = \frac{\omega_p}{2}$, so that the TPA depends only on the transverse signal and idler wave vectors. Next, we apply the Schmidt decomposition to $F(\mathbf{q}_s,\mathbf{q}_i)$, which is not simple if the full dimensionality is taken into account. The Schmidt decomposition can be made explicitly in the cylindrical frame of reference or by using the double-Gauss approximation [21–23] in the Cartesian frame. In the latter case the sinc factor in (2) is approximated by a Gaussian function and then the TPA can be factorized in two terms, each one depending only on x or y components of $\mathbf{q}_s,\mathbf{q}_i$. Using analytical Schmidt decomposition in each direction, we obtain the total decomposition of the TPA $F(\mathbf{q}_s,\mathbf{q}_i)$ (Appendix A). Here we focus on the explicit Schmidt decomposition in the cylindrical frame of reference, in which each transverse wave vector is given by its absolute value $q_{i,s}$ and azimuthal angle $\phi_{i,s}$. Then, $F(\mathbf{q}_s,\mathbf{q}_i)$ can be written as a Fourier expansion due to its periodicity in $(\phi_s-\phi_i)$ [24],

$$F(q_s,q_i,\phi_s-\phi_i) = \sum_n \chi_n(q_s,q_i) e^{in(\phi_s-\phi_i)}, \tag{3}$$

where $\chi_n(q_s,q_i)$ can be found using the inverse Fourier transform. Then, the one-dimensional (1D) Schmidt decomposition yields

$$\chi_n(q_s,q_i) = \sum_m \sqrt{\lambda_{mn}} \frac{u_{mn}(q_s)}{\sqrt{q_s}} \frac{v_{mn}(q_i)}{\sqrt{q_i}}, \tag{4}$$

with the functions $u_{mn}(q_s)$ and $v_{mn}(q_i)$ obeying the normalization condition,

$$\int_0^\infty dq_s u_{mn}(q_s) u^*_{kn}(q_s) = \int_0^\infty dq_i v_{mn}(q_i) v^*_{kn}(q_i) = \delta_{mk}.$$

Decomposition (4) allows one to expand the TPA as

$$F(\mathbf{q}_s,\mathbf{q}_i) = \sum_{m,n} \sqrt{\lambda_{mn}} \frac{u_{mn}(q_s)}{\sqrt{q_s}} \frac{v_{mn}(q_i)}{\sqrt{q_i}} e^{in(\phi_s-\phi_i)}. \tag{5}$$

Using Eq. (5), we rewrite the Hamiltonian (1) in terms of the photon creation/annihilation operators for the new collective spatial Schmidt modes,

$$H = i\hbar\Gamma \sum_{m,n} \sqrt{\lambda_{mn}} (A^\dagger_{mn} B^\dagger_{mn} - A_{mn} B_{mn}), \tag{6}$$

where

$$A^\dagger_{mn} = \int d\mathbf{q}_s \frac{u_{mn}(q_s)}{\sqrt{q_s}} e^{in\phi_s} a^\dagger_{\mathbf{q}_s}, \quad B^\dagger_{mn} = \int d\mathbf{q}_i \frac{v_{mn}(q_i)}{\sqrt{q_i}} e^{-in\phi_i} a^\dagger_{\mathbf{q}_i}, \tag{7}$$

with $d\mathbf{q} = q dq d\phi$.

The performed procedure is the generalized Bloch-Messiah reduction, which in the frequency domain introduces new collective photon operators and collective modes sometimes called broadband modes [13,14].

By passing to the new operators, we diagonalize the Hamiltonian (6), so that the new modes are coupled pairwise. Note that the new operators obey standard commutation relations:

$$[A_{mn}, A^\dagger_{kl}] = \delta_{mk}\delta_{nl}, \quad [A_{mn}, B^\dagger_{kl}] = \delta_{mk}\delta_{n,-l}. \tag{8}$$

The last relation results from the nondistinguishability of the signal and idler photons, manifested in the invariance of the TPA (2) to the $\mathbf{q}_s \longleftrightarrow \mathbf{q}_i$ exchange. Further, we take this into account by setting $u_{mn}(\xi) = v_{mn}(\xi)$.

The Heisenberg equations for the Schmidt-mode operators have the form

$$\frac{dA_{mn}}{dt} = \Gamma\sqrt{\lambda_{m,n}}(A^\dagger_{m,-n} + B^\dagger_{mn}) = 2\Gamma\sqrt{\lambda_{mn}} B^\dagger_{mn}, \quad \frac{dB^\dagger_{mn}}{dt} = \Gamma\sqrt{\lambda_{m,n}}(A_{mn} + B_{m,-n}) = 2\Gamma\sqrt{\lambda_{mn}} A_{mn}. \tag{9}$$

Here we used the relation $A^\dagger_{m,-n} = B^\dagger_{mn}$, $A_{mn} = B_{m,-n}$, $\lambda_{mn} = \lambda_{m,-n}$.

The solutions are given by the Bogolyubov-type transformations,

$$A^{\text{out}}_{mn} = A^{in}_{mn}\cosh[G\sqrt{\lambda_{mn}}] + [B^{in}_{mn}]^\dagger \sinh[G\sqrt{\lambda_{mn}}], \quad B^{\text{out}}_{mn} = B^{in}_{mn}\cosh[G\sqrt{\lambda_{mn}}] + [A^{in}_{mn}]^\dagger \sinh[G\sqrt{\lambda_{mn}}],$$

where $G \equiv \int 2\Gamma dt$ is the parametric gain and A^{in}_{mn}, B^{in}_{mn} are the initial (vacuum) photon annihilation operators in the corresponding Schmidt mode (7). Because in experiment one usually deals with plane-wave modes, visualized, for instance, in the focal plane of a lens, it is useful to obtain explicit expressions for the plane-wave photon creation and annihilation operators of the signal and idler beams. We do this analytically by expanding them over the set of orthogonal normalized Schmidt modes, and the explicit expressions for $a^\dagger_{\mathbf{q}_s}$, $a^\dagger_{\mathbf{q}_i}$ are given in Appendix B. Further, we calculate all the observables using these plane-wave operators.

Mean values of photon numbers and their second-order moments are found by averaging over the vacuum state,

$$\langle N_s(\mathbf{q}_s)\rangle = \langle 0|a^\dagger_{\mathbf{q}_s} a_{\mathbf{q}_s}|0\rangle, \tag{10}$$

and similarly for $\langle N_s^2(\mathbf{q}_s)\rangle$ and $\langle N_s(\mathbf{q}_s)N_i(\mathbf{q}_i)\rangle$.

The obtained photon-number distributions for the signal and idler beams take the form

$$\langle N_{s,i}(\mathbf{q}_{s,i})\rangle = \sum_{mn} \frac{|u_{mn}(q_{s,i})|^2}{q_{s,i}} (\sinh[G\sqrt{\lambda_{mn}}])^2. \tag{11}$$

This means that the Schmidt modes contribute to the total photon number incoherently, with the weights

$$\lambda'_{mn} = \frac{(\sinh[G\sqrt{\lambda_{mn}}])^2}{\sum_{mn}(\sinh[G\sqrt{\lambda_{mn}}])^2}, \tag{12}$$

which can be understood as the new Schmidt eigenvalues, renormalized at high gain. At low gain, $G \ll 1$, $\lambda'_n = \lambda_n$.

Finally, one can calculate the variance of the photon-number difference in the signal and idler beams, $\mathrm{Var}(N_s - N_i) \equiv \langle (N_s - N_i)^2\rangle - \langle N_s - N_i\rangle^2$, the correlation function $G^{(2)}_{is} \equiv \langle N_s N_i\rangle$, its normalized version, and any other statistical values (Appendix B).

The expression for the TPA (2) can be generalized for more complicated experimental schemes. Our approach is valid whenever the TPA is periodic in $(\phi_s - \phi_i)$. Further, we apply our model to the description of three different experiments.

III. ANGULAR DISTRIBUTIONS OF INTENSITY AND CORRELATIONS

BSV was generated by pumping a collinear degenerate type-I traveling-wave optical parametric amplifier (OPA) with the third harmonic of a Nd:YAG laser [wavelength 354.7 nm, repetition rate 1 kHz, pulse width 18 ps, and mean power 20 mW, see Fig. 1(a)]. The Gaussian pump beam was focused into a pair of 3 mm BBO crystals by means of a lens system (L_1,L_2) that reduced the waist diameter to 120 μm FWHM. The crystals were oriented in the anisotropy-compensating configuration, that is, with the optic axes in the same plane but tilted at opposite angles to the pump [25,26], and placed at a distance of 7 mm. The TPA corresponding to this experimental setup can be found in Eq. (A1). The pump was removed by means of a dichroic mirror (DM) and a red glass filter (RG645). An interference filter (IF) selected the radiation bandwidth of 10 nm around 710 nm. The 2D spatial spectra of BSV were recorded by a CCD camera placed in the focal plane of a lens L (focal length $f = 100$ mm), placed, in its turn, at a distance f from the second crystal. The Cartesian coordinate in the plane of the CCD camera corresponded to the external scattering angle θ as $x = f\theta$. For comparing the theoretical predictions with the measured intensity distributions and variances of the photon-number differences, we made a cut of the 2D spectrum along the axis orthogonal to the principal plane of the crystal [white dashed line in Fig. 1(a)]. The profile of the spectrum along this axis [Fig. 1(b)] was close to Gaussian. However, according to the calculation, it still contained $K = 1.9$ angular modes in the x dimension.

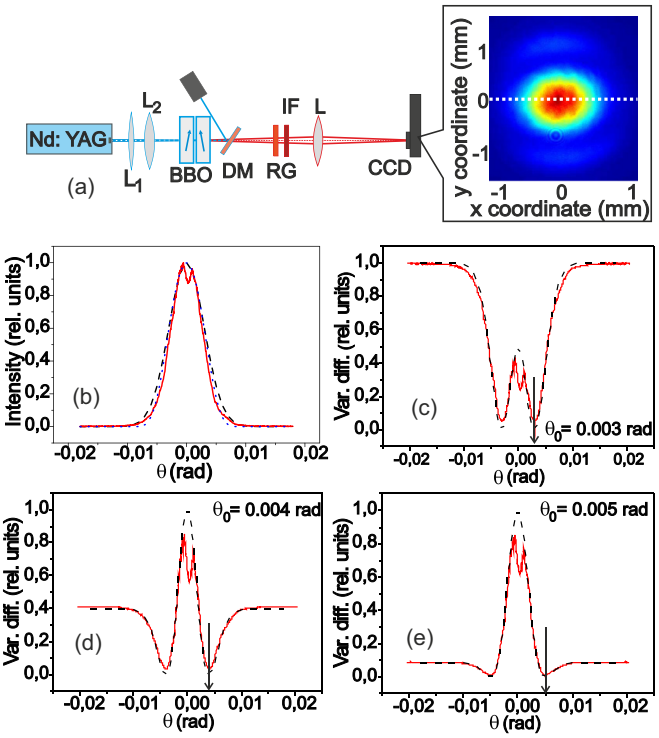

FIG. 1. (Color online) The setup used for the study of BSV angular spectra and a typical 2D image on the CCD camera, with the white dashed line showing (a) the direction of the 1D scan, (b) the measured and calculated intensity angular distributions, and the measured and calculated angular distributions of the photon-number difference variance with the angle θ_0 fixed at (c) 3 mrad, (d) 4 mrad, and (e) 5 mrad, shown with arrows. Red solid lines: experiment, black dashed lines: theory.

For all obtained angular distributions, a certain angle θ_0 was fixed, and the difference between the CCD signals corresponding to this angle and to all other angles θ was calculated, $S(\theta) - S(\theta_0)$. The variance of this difference is a measure of intensity correlations between different plane-wave modes. Using an ensemble of 4000 frames, this variance was measured as a function of θ for several θ_0. The obtained plots were normalized to the maximum of the distribution and compared with the theory. Figure 1 shows three cases with different θ_0. In red, the experimental values are presented and in black, the theoretical fits. Similarly to the measurements performed for frequency spectra in Ref. [27], each distribution should contain, in the general case, two dips and a peak. The right-hand dip at the chosen angle θ_0 shows the reduced noise in the difference intensity due to the autocorrelation, which would also appear in thermal light. The left-hand dip corresponds to the cross correlation between the intensities in the signal and idler plane-wave modes. Therefore it is symmetric to the right-hand one. The peak shows excess fluctuations due to the superbunching behavior of collinear frequency-degenerate BSV [28].

IV. DEPENDENCE ON THE PARAMETRIC GAIN

According to Eq. (12), the increase in G should lead to a redistribution of the Schmidt eigenvalues. Low-order ones

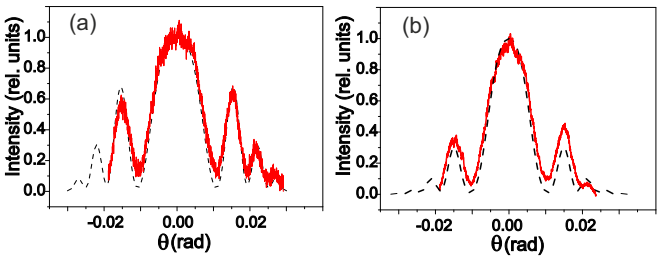

FIG. 2. (Color online) Normalized angular spectra (red solid line) of PDC for two 1 mm crystals separated by 3 mm measured at the pump powers (a) 29 mW and (b) 73 mW. The corresponding theoretical fits (black dashed lines) are calculated for gain values $G = 2.1$ and $G = 3.3$.

have higher values and should get enhanced, while high-order ones should get suppressed. This leads to the reduction in the effective mode number (Schmidt number),

$$K = \left[\sum_n \lambda_n'^2\right]^{-1}. \tag{13}$$

The reduction in the number of modes naturally leads to the reshaping of the spectrum. Indeed, we measured the angular intensity distributions at different values of the parametric gain. For this experiment, we used thinner crystals (1 mm), which led to a larger mode number and a more complicated structure of the spectrum due to the interference of radiation from two separated crystals [29].

Figure 2 shows 1D angular spectra obtained for two different pump powers, 29 mW and 73 mW. The positions of the minima and the maxima, given by the phase delays in the crystals and in the gap between them, do not depend on the power but the shapes of the peaks are strongly affected by it. At lower power, the side peaks are more pronounced and the central one is considerably broader than at high power. The observed shape is in agreement with the theory (black dashed lines). Both theory and experiment show the reduction of side peaks in the spectrum, as well as the narrowing of the central peak, with the gain increase. This indirectly confirms the reduction in the number of modes. A direct calculation of the Schmidt number (13) shows that it indeed decreases with the value of the parametric gain [Fig. 3(a)]. This is in agreement with the measurement made by Allevi and Bondani [30] who observed a reduction in the Schmidt number in the range of pump powers below the depletion range. We have also calculated the angular width of the intensity covariance (defined in Appendix B) versus the parametric gain [Fig. 3(b)]. The FWHM of the covariance increases with the parametric gain, as observed by Brida *et al.* [31] and Allevi *et al.* [32]. However it appears to be limited by the size of the lowest Schmidt mode, which is the only one that remains in the high-gain limit.

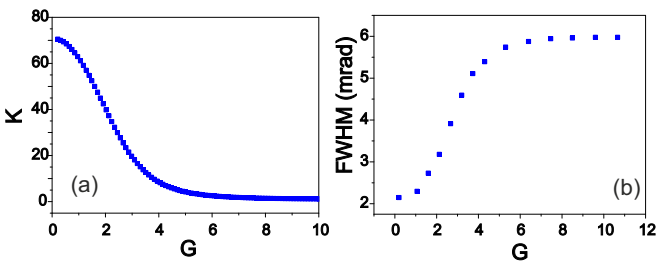

FIG. 3. (Color online) (a) The Schmidt number K and (b) the width of the covariance versus the parametric gain for the same experimental configuration as in Fig. 2.

V. TRANSVERSE WALKOFF AND ITS COMPENSATION

Finally, our model provides the description of PDC in the presence of spatial walkoff. Interestingly, manifestations of spatial walkoff at low gain and high gain are very different. While at low gain, walkoff leads only to the asymmetry of angular spectra and an increase in the number of modes [22,26], at high gain it can create two separate angular peaks in the geometry where collinear PDC is expected [25]. The results of calculation are presented in Fig. 4. We consider two 1 mm BBO crystals oriented for collinear frequency-degenerate phase matching and placed at a distance 8 mm into a pump beam with the waist FWHM 35 μm. For calculation details, see Appendix C. At low gain and the crystals' optic axes parallel [Fig. 4(a)], spatial walkoff leads to a strong asymmetry of the spectrum while the interference of emission from different crystals creates fringes. These fringes are more pronounced on the side opposite to the walk-off direction due to the induced coherence effect [25,33]: the radiation propagating along the pump Poynting vector from both crystals is indistinguishable, hence we see interference at matching angles. Placing a second crystal with the optic axis tilted symmetrically [Fig. 4(b)] symmetrizes the spectrum but does not eliminate the fringes [26].

At high gain [Figs. 4(c) and 4(d)], the spectra of the two crystals with parallel axes in the same collinear degenerate

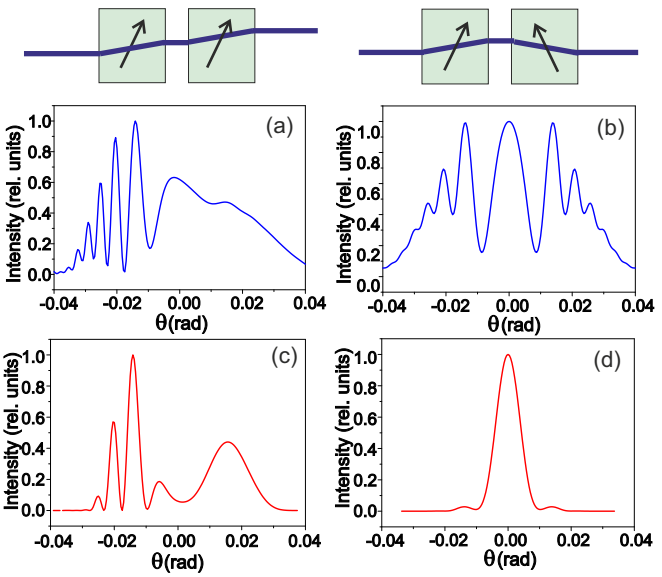

FIG. 4. (Color online) Angular spectra of PDC from two crystals with (a), (c) the axes parallel and (b), (d) tilted symmetrically with respect to the pump calculated for the gain values (a), (b) 10^{-4} and (c), (d) 10. On top, the crystals configurations are shown.

orientation show two peaks of emission, as observed in Ref. [25]. Our calculation reproduces these two peaks, as well as the interference fringes on one of them [Fig. 4(c)]. The peaks are due to the fact that at high gain, amplification occurs primarily along the pump Poynting vector as well as in the direction of the twin beam. In the compensating configuration, at high gain no more interference fringes are observed, as seen in Fig. 4(d), and strong amplification occurs in the direction collinear to the pump wave vector. The experimental distribution for a similar case is shown in Fig. 1(b) and is in agreement with the calculation.

VI. CONCLUSION

In conclusion, we have presented an analytical description of the spatial properties of BSV generated via PDC or FWM. Our theory is applicable for both low-gain and high-gain regimes and is based on the collective (Schmidt) modes whose contributions, strongly depending on the gain, are responsible for the spatial intensity distribution of the generated state and arising multiphoton correlations. Certainly, it is not always possible to calculate analytically the modes; however, this is a different problem. As long as the Schmidt modes are known, all the measurable quantities can be found analytically. The model explains several effects observed for BSV, such as the change of the multiphoton correlations and the mode content with the parametric gain, the interference effects in a two-crystal scheme for BSV generation and, finally, the effect of spatial walkoff. The concept of collective independent modes, analogous to the normal modes of coupled oscillators, bridges the continuous- and discrete-variable formalisms and gives a deep insight into the general physical nature of multiple correlations in strongly coupled multipartite systems.

ACKNOWLEDGMENTS

The research leading to these results received funding from the EU FP7 under Grant Agreement No. 308803 (Project BRISQ2). We also acknowledge partial financial support of the Russian Foundation for Basic Research, Grants No. 14-02-31084 mol-a and No. 14-02-00389-a. P.R.Sh acknowledges support of the 'Dynasty' foundation. We thank F. Miatto for helpful discussions.

APPENDIX A: TWO-CRYSTAL SCHEME

In all experiments described above, PDC is obtained by placing two crystals one after another, usually with the optic axes tilted symmetrically with respect to the pump direction. Such a configuration, used already in the early papers on squeezing [34], allows one to reach high parametric gain without strong walk-off effect. However, the description of the two-dimensional spatial spectrum of its PDC emission has been never done before.

The two-crystal case is more complicated to describe than the single-crystal one. The latter, under certain conditions, allows the two-photon amplitude (TPA) to be written in the double-Gauss approximation and further factored in two one-dimensional distributions. In the two-crystal case, due to the interference between the radiation from different crystals,

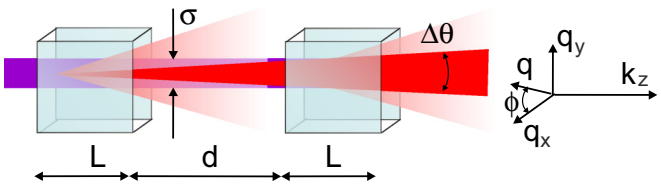

FIG. 5. (Color online) The two-crystal scheme and the basic notation. The angular width of radiation from the first crystal amplified in the second crystal, $\Delta\theta$, is determined by the ratio $\sigma/(2L+d)$, where σ characterizes the pump width, L is the crystal length and d the distance between the crystals. The transverse components of the wave vectors are denoted by $\mathbf{q}$.

the TPA contains multiple maxima and minima and therefore cannot be described within the framework of the double-Gauss model. Moreover, the geometry obviously has cylindrical symmetry and does not allow factorization of the TPA in the horizontal and vertical parts. This immediately dictates using the Laguerre-Gauss basis for the TPA Schmidt decomposition.

The two-crystal scheme we consider is shown in Fig. 5. Two crystals of length L are separated by an air gap of length d and pumped by a Gaussian pump with the beam waist described by the parameter σ. The full width at half maximum (FWHM) of the pump intensity distribution, $2\sqrt{\ln 2}\sigma$, is assumed to be much larger than the transverse walk-off distance in a single crystal. This allows one to neglect the transverse walkoff and makes the system cylindrically symmetric. We also assume frequency degeneracy, i.e., that the signal and idler frequencies are equal to $\omega_s = \omega_p/2$, with ω_p denoting the frequency of the pump.

The TPA $F(\mathbf{q}_s,\mathbf{q}_i)$ for this scheme can be written in the form [24,29,35]

$$F(\mathbf{q}_s,\mathbf{q}_i) = C\exp\left\{-\frac{\sigma^2(\mathbf{q}_s+\mathbf{q}_i)^2}{2}\right\}\mathrm{sinc}\left(\frac{L(\mathbf{q}_s-\mathbf{q}_i)^2}{4k_p}\right) \times \cos\left(\frac{L(\mathbf{q}_s-\mathbf{q}_i)^2}{4k_p}+\frac{\delta n k_s d}{n_s} + \frac{d\left(\mathbf{q}_s^{\mathrm{air}}-\mathbf{q}_i^{\mathrm{air}}\right)^2}{4k_p^{\mathrm{air}}}\right)\exp\left\{i\left(\frac{L(\mathbf{q}_s-\mathbf{q}_i)^2}{2k_p} + \frac{\delta n k_s d}{n_s}+\frac{d\left(\mathbf{q}_s^{\mathrm{air}}-\mathbf{q}_i^{\mathrm{air}}\right)^2}{4k_p^{\mathrm{air}}}\right)\right\}, \tag{A1}$$

where C is the normalization constant, $k_{p,s}^{\mathrm{air}} = n_{p,s}^{\mathrm{air}}\frac{\omega_{p,s}}{c}$, $n_{p,s,i}^{\mathrm{air}}$ are the refractive indices for the pump, signal and idler radiation in the air gap between the crystals, $\delta n = n_p^{\mathrm{air}} - \frac{1}{2}(n_s^{\mathrm{air}}+n_i^{\mathrm{air}})$ and $\mathbf{q}_{s,i}^{\mathrm{air}}(\mathbf{q}_{s,i})$ are the transverse components of the wave vectors of the signal and idler beams in the air gap (crystal). In the cylindrical frame of reference, they are characterized by their absolute values $q_{s,i}$ and azimuthal angles $\phi_{s,i}$: $\mathbf{q}_{s,i} = (q_{s,i},\phi_{s,i})$. For small angles of emission, $\frac{(\mathbf{q}_s^{\mathrm{air}}-\mathbf{q}_i^{\mathrm{air}})^2}{4k_p^{\mathrm{air}}} \approx n_s\frac{(\mathbf{q}_s-\mathbf{q}_i)^2}{4k_p}$. In this case the TPA (A1) depends on four polar coordinates describing the transverse wave vectors of the signal and idler beams. The key point of the cylindrical symmetry is that the TPA depends not separately on the angles ϕ_s and ϕ_i but only on their difference $(\phi_s-\phi_i)$. This

immediately enables an explicit Schmidt decomposition of the TPA as it was described in Eqs. (3) and (4).

At the same time, in the Cartesian frame of reference the explicit Schmidt decomposition can hardly be performed in full dimensionality. For this reason different approximations should be used to simplify this procedure. One of them is appropriate if the distance between the crystals is small compared to the period of the interference pattern observed when one of the crystals is moved (36 mm [29]), then the approximation of a single crystal of double length can be used. In this case, the double-Gauss approximation can be applied and the Schmidt decomposition of the TPA can be provided separately in each (x or y) direction. This method is described below in Appendix C. Another simplification is appropriate if the anisotropy plays an important role. In such a case only a single dimension needs to be considered, the one in which the spatial walkoff takes place. Whenever all important effects are associated with anisotropy they can be taken into account under such 1D approximation. Thus the problem of the Schmidt decomposition can be solved by different means, and as soon as it is solved, our analytical approach leads straightforwardly to the final results. Thus our method based on collective Schmidt modes is suitable for different experimental schemes.

APPENDIX B: PLANE-WAVE SOLUTIONS

In the general case, the Schmidt decomposition of the TPA (A1) can be performed in the cylindrical frame of reference taking into account that $\mathbf{q}_s\mathbf{q}_i = q_s q_i \cos(\phi_s - \phi_i)$ and using the fact that the TPA depends only on the difference $\phi_s - \phi_i$ and this dependence is periodic. Such a feature is a direct consequence of the azimuthal symmetry of PDC radiation in the scheme we use and leads to the invariance of the radiation intensity to the azimuthal angle. Under these conditions it is possible to introduce new collective photon creation operators $A^\dagger_{mn}$, $B^\dagger_{mn}$ (7). These operators are responsible for the creation of a photon in a certain Schmidt mode characterized by its own spatial distribution. Since usually the description not only in terms of the Schmidt modes but also in the framework of plane-wave operators is needed, further we find the solution for these operators and calculate some measurable quantities. Using the expression for the Hamiltonian in terms of $A^\dagger_{mn}$ and $B^\dagger_{mn}$ given by Eq. (7), the Heisenberg equation for plane-wave operators $a_{s,i}$ can be written in the form

$$\frac{da_{\mathbf{q}_{s,i}}}{dt} = \Gamma \sum_{mn} \sqrt{\lambda_{mn}} \frac{u_{mn}(q_{s,i})}{\sqrt{q_{s,i}}} [A^\dagger_{mn} e^{-in\phi_{s,i}} + B^\dagger_{mn} e^{in\phi_{s,i}}]. \tag{B1}$$

Here we use the fact that $u_{mn}(\xi) = v_{mn}(\xi)$ due to the invariance of TPA (A1) to the $\mathbf{q_s} \leftrightarrow \mathbf{q_i}$ exchange.

With an account for the time-dependent expression of the Schmidt-mode operators $A^\dagger_{mn}$, $B^\dagger_{mn}$, after introducing $S_{mn}(\phi) \equiv \frac{1}{2}[B^{in}_{mn} e^{-in\phi} + A^{in}_{mn} e^{in\phi}]$ we obtain the solution to (B1) in the form

$$a^{\text{out}}_{\mathbf{q}_{s,i}} = a^{in}_{\mathbf{q}_{s,i}} + \sum_{mn} \frac{u_{mn}(q_{s,i})}{\sqrt{q_{s,i}}} [S^\dagger_{mn}(\phi_{s,i}) \sinh(\sqrt{\lambda_{mn}} G) + S_{mn}(\phi_{s,i})(\cosh(\sqrt{\lambda_{mn}} G) - 1)]. \tag{B2}$$

From this solution, we calculate the mean photon number, for example, for the signal beam by averaging $[a^{\text{out}}_{\mathbf{q}_s}]^\dagger a^{\text{out}}_{\mathbf{q}_s}$ over the vacuum state:

$$\langle N_s(\mathbf{q}_s) \rangle = \sum_{mn} \frac{|u_{mn}(q_s)|^2}{q_s} (\sinh[G\sqrt{\lambda_{mn}}])^2. \tag{B3}$$

We also calculate the covariance of the photon numbers,

$$\text{Cov}(\text{N}_\text{s}(\mathbf{q}_\text{s}),\text{N}_\text{i}(\mathbf{q}_\text{i})) = \langle N_s(\mathbf{q}_s) N_i(\mathbf{q}_i) \rangle - \langle N_s(\mathbf{q}_s) \rangle \langle N_i(\mathbf{q}_i) \rangle. \tag{B4}$$

It should be emphasized that while the Schmidt modes depend on the azimuthal angles of signal and idler photons, the mean photon numbers demonstrate independence of them. At the same time, the covariance depends on the combination $(\phi_s - \phi_i)$, which evidently shows correlation between the signal and idler photons with transverse wave vectors of the same or opposite directions [$\cos(\phi_s - \phi_i) = 0, \pi$, corresponding to autocorrelations and cross correlations, respectively]:

$$\begin{aligned}
\text{Cov}(\text{N}_\text{s}(\mathbf{q}_\text{s}),\text{N}_\text{i}(\mathbf{q}_\text{i})) = {} & \left| \sum_{mn} \frac{v_{mn}(q_i) u_{mn}(q_s)}{\sqrt{q_i q_s}} \sinh[\sqrt{\lambda_{mn}} G](\cosh[\sqrt{\lambda_{mn}} G] - 1) \cos[n(\phi_s - \phi_i)] \right|^2 \\
& + 2\text{Re} \left[\sum_{mn} \frac{v^*_{mn}(q_i) u^*_{mn}(q_s)}{\sqrt{q_i q_s}} \sinh[\sqrt{\lambda_{mn}} G](\cosh[\sqrt{\lambda_{mn}} G] - 1) \cos[n(\phi_s - \phi_i)] \sum_{mn} \frac{v_{mn}(q_i) u_{mn}(q_s)}{\sqrt{q_i q_s}} \right. \\
& \left. \times \sinh[\sqrt{\lambda_{mn}} G] \cos[n(\phi_s - \phi_i)] \right] + \left| \sum_{mn} \frac{v_{mn}(q_i) u_{mn}(q_s)}{\sqrt{q_i q_s}} \sinh[\sqrt{\lambda_{mn}} G] \cos[n(\phi_s - \phi_i)] \right|^2 \\
& + \sum_{mn} \frac{|v_{mn}(q_i)|^2 |u_{mn}(q_s)|^2}{q_i q_s} (\sinh[\sqrt{\lambda_{mn}} G])^4 (1 + 2\cos[2n(\phi_s - \phi_i)]) \\
& + \left| \sum_{mn} \frac{v^*_{mn}(q_i) u_{mn}(q_s)}{\sqrt{q_i q_s}} (\sinh[\sqrt{\lambda_{mn}} G])^2 \cos[n(\phi_s - \phi_i)] \right|^2 .
\end{aligned} \tag{B5}$$

However, if only emission within a certain plane is analyzed (which can be achieved in experiment by using a horizontal or a vertical slit in front of the CCD or using only a single vertical or horizontal row of the CCD pixels), the covariance

takes a simpler form and depends on only two variables q_s and q_i.

APPENDIX C: CARTESIAN FRAME AND DOUBLE-GAUSS APPROXIMATION

The general expression (A1) for TPA cannot be written as a product of one-dimensional TPAs in the Cartesian frame of reference, for instance one depending on the x and the other one depending on the y wave vector components. Because of this, the problem can be solved analytically only under some approximations.

For instance, if the distance between the two crystals is small and the crystals have optic axes tilted oppositely, one can consider such a system as one crystal of double length. Then the double-Gauss approximation, in which the sinc term of the TPA is approximated by a Gaussian function with suited parameters, can be used. The amplitude can then be factored in two terms, each one depending only on the x or y components of $\mathbf{q}_s$ and $\mathbf{q}_i$,

$$F(\mathbf{q}_s,\mathbf{q}_i) = F_1(q_{sx},q_{ix})F_2(q_{sy},q_{iy}). \tag{C1}$$

In this case, the Schmidt decomposition for x and y directions can be provided independently on each other,

$$F(\mathbf{q}_s,\mathbf{q}_i) = \sum_n \sqrt{\lambda_n}u_n(q_{sx})v_n(q_{ix}) \times \sum_m \sqrt{\tilde{\lambda}_m}\tilde{u}_m(q_{sy})\tilde{v}_m(q_{iy}). \tag{C2}$$

As a result, the TPA can be represented as the decomposition in two-dimensional Schmidt modes, $U_{nm}(\mathbf{q}_s) = u_n(q_{sx})\tilde{u}_m(q_{sy})$, $V_{nm}(\mathbf{q}_i) = v_n(q_{ix})\tilde{v}_m(q_{iy})$, depending on the signal or idler variables only:

$$F(\mathbf{q}_s,\mathbf{q}_i) = \sum_{nm}\sqrt{\lambda_n\tilde{\lambda}_m}U_{nm}(\mathbf{q}_s)V_{nm}(\mathbf{q}_i). \tag{C3}$$

It should be noticed that since the anisotropy is not taken into account and the pump is axially symmetric, the eigenmodes and eigenvalues for x and y directions are identical:

$$u_n(\xi) = \tilde{u}_n(\xi), \quad v_n(\xi) = \tilde{v}_n(\xi), \quad \lambda_n = \tilde{\lambda}_n. \tag{C4}$$

Then we can introduce new collective photon creation operators $A^\dagger_{mn}$, $B^\dagger_{mn}$,

$$A^\dagger_{mn} = \int d\mathbf{q}_s U_{mn}(\mathbf{q}_s)a^\dagger_{\mathbf{q}_s}, \qquad B^\dagger_{mn} = \int d\mathbf{q}_i V_{mn}(\mathbf{q}_i)a^\dagger_{\mathbf{q}_i}, \tag{C5}$$

which provide the diagonalization of the initial Hamiltonian and allow one to obtain the time-depending solution not only for Schmidt modes but also for the plane-wave operators. From the expressions obtained for the plane-wave operators, we can calculate the mean photon number, as well as the variance of the photon-number difference in the signal and idler beams, $\mathrm{Var}(N_s - N_i) \equiv \langle (N_s - N_i)^2\rangle - \langle N_s - N_i\rangle^2$, the correlation function $G^{(2)}_{is} \equiv \langle N_s N_i\rangle$, and its normalized value, $g^{(2)}_{is} \equiv \frac{G^{(2)}_{is}}{\langle N_s\rangle\langle N_i\rangle}$. In full dimensionality the mean number of photons for the signal beam (and similarly for the idler beam) takes the form

$$N_s(q_{sx},q_{sy}) = \sum_{nm}|u_n(q_{sx})|^2|u_m(q_{sy})|^2(\sinh[\sqrt{\lambda_n\lambda_m}G])^2. \tag{C6}$$

But if only one-dimensional distribution is analyzed in experiment by fixing $q_{iy} = q_{sy} = 0$ (using a slit), it is given by

$$N_s(q_{sx}) = \sum_{nm}|u_n(q_{sx})|^2|u_m(0)|^2(\sinh[\sqrt{\lambda_n\lambda_m}G])^2. \tag{C7}$$

Moreover, in the case when the number of modes is sufficiently small and consequently their weights drop sharply with the increase of m (which was realized in experiment), one can restrict the sum over m to only the first term and the expression for the photon number takes a simpler form,

$$N_s(q_{sx}) = \sum_{n}|u_n(q_{sx})|^2|u_0(0)|^2(\sinh[\sqrt{\lambda_n\lambda_0}G])^2. \tag{C8}$$

Under such conditions the variance of the photon number difference can be represented as

$$\mathrm{Var}(N_s - N_i) = \mathrm{Var}(N_s) + \mathrm{Var}(N_i) - 2\mathrm{Cov}(N_s,N_i), \tag{C9}$$

where

$$\mathrm{Var}(N_s) = |u_0(0)|^4\Big(\Big|\sum u_n u_n \sinh[\Lambda_n](\cosh[\Lambda_n]-1)\Big|^2 + 2\mathrm{Re}\Big[\sum u_n^* u_n^* \sinh[\Lambda_n](\cosh[\Lambda_n]-1)\sum u_n u_n \sinh[\Lambda_n]\Big] + \Big|\sum u_n u_n \sinh[\Lambda_n]\Big|^2 + \Big|\sum u_n^* u_n(\sinh[\Lambda_n])^2\Big|^2 + 3\sum |u_n|^2|u_n|^2(\sinh[\Lambda_n])^4\Big) + |u_0(0)|^2\langle N_s\rangle, \tag{C10}$$

$$\mathrm{Var}(N_i) = |v_0(0)|^4\Big(\Big|\sum v_n v_n \sinh[\Lambda_n](\cosh[\Lambda_n]-1)\Big|^2 + 2\mathrm{Re}\Big[\sum v_n^* v_n^* \sinh[\Lambda_n](\cosh[\Lambda_n]-1)\sum v_n v_n \sinh[\Lambda_n]\Big] + \Big|\sum v_n v_n \sinh[\Lambda_n]\Big|^2 + \Big|\sum v_n^* v_n(\sinh[\Lambda_n])^2\Big|^2 + 3\sum |v_n|^2|v_n|^2(\sinh[\Lambda_n])^4\Big) + |v_0(0)|^2\langle N_i\rangle, \tag{C11}$$

$$\mathrm{Cov}(N_s,N_i) = |u_0(0)|^2|v_0(0)|^2\Big(\Big|\sum v_n u_n \sinh[\Lambda_n](\cosh[\Lambda_n]-1)\Big|^2 + 2\mathrm{Re}\Big[\sum v_n^* u_n^* \sinh[\Lambda_n](\cosh[\Lambda_n]-1)\sum v_n u_n \sinh[\Lambda_n]\Big] + \Big|\sum v_n u_n \sinh[\Lambda_n]\Big|^2 + \Big|\sum v_n^* u_n(\sinh[\Lambda_n])^2\Big|^2 + 3\sum |v_n|^2|u_n|^2(\sinh[\Lambda_n])^4\Big), \tag{C12}$$

with $u_n = u_n(q_{sx}), v_n = v_n(q_{ix})$ and $\Lambda_n = G\sqrt{\lambda_n \lambda_0}$. It should be noticed that this approximation works rather well for two closely placed crystals. Indeed, the theoretical results obtained by such a way fit very well the experimental curves (see Fig. 1).

APPENDIX D: ANISOTROPY EFFECT

If the pump diameter is small, or the crystal is long, it is necessary to take into account the spatial walkoff. This breaks down the axial symmetry of the problem. However, in some cases, it is enough to take into account not the full two-dimensional angular spectra but only a single dimension. For instance, when the walk-off effect is described, it is sufficient to consider only the plane of the optic axis. The corresponding TPA is described by the expression obtained in Ref. [25] but including nonzero distance between the crystals. For the compensating geometry, in which the two crystals have optic axes tilted oppositely, the TPA can be written as

$$F(\theta_s,\theta_i) = \exp\left[-\frac{\sigma^2(\Delta_\perp \cos\rho + \Delta_\parallel \sin\rho)^2}{2}\right]\exp\left[-i\frac{L}{2}\xi\right] \times \operatorname{sinc}\left[\frac{L}{2}\xi\right] + \exp\left[-\frac{\sigma^2(\Delta_\perp \cos\rho - \Delta_\parallel \sin\rho)^2}{2}\right] \times \exp\left[i\frac{L}{2}\eta\right]\operatorname{sinc}\left[\frac{L}{2}\eta\right]\exp[i(L\Delta_\parallel + d\Delta_\parallel^{\text{air}})], \tag{D1}$$

where ρ is the walk-off angle, $\Delta_\parallel = k_p - k_s\cos\theta_s - k_i\cos\theta_i$ and $\Delta_\parallel^{\text{air}} = k_p^{\text{air}} - k_s^{\text{air}}\cos(n_s\theta_s) - k_i^{\text{air}}\cos(n_i\theta_i)$ are longitudinal mismatches in the crystal and in the air gap, respectively, $\Delta_\perp = k_s\sin\theta_s + k_i\sin\theta_i$ is the transverse mismatch, $\xi = \Delta_\parallel - \Delta_\perp\tan\rho$, $\eta = \Delta_\parallel + \Delta_\perp\tan\rho$.

For noncompensating geometry, in which the optic axes are parallel in both crystals, we have

$$F(\theta_s,\theta_i) = \exp\left[-\frac{\sigma^2(\Delta_\perp \cos\rho + \Delta_\parallel \sin\rho)^2}{2}\right] \times \exp\left[-i\frac{L}{2}\xi\right]\operatorname{sinc}\left[\frac{L}{2}\xi\right] + \exp\left[-\frac{\sigma^2(\Delta_\perp \cos\rho + \Delta_\parallel \sin\rho)^2}{2}\right] \times \exp\left[-i\frac{L}{2}\xi\right]\operatorname{sinc}\left[\frac{L}{2}\xi\right]\exp[i(L\Delta_\parallel + d\Delta_\parallel^{\text{air}})]. \tag{D2}$$

In this case, the one-dimensional approximation reflects the main features of the system and allows one to describe the behavior of the signal not only qualitatively but also quantitatively. Nevertheless, the consideration in full dimensionality without any approximations remains an important but difficult problem and will be a subject of our further investigation.

[1] T. Sh. Iskhakov, I. N. Agafonov, M. V. Chekhova, and G. Leuchs, Phys. Rev. Lett. **109**, 150502 (2012).
[2] I. N. Agafonov, M. V. Chekhova, and G. Leuchs, Phys. Rev. A **82**, 011801 (2010).
[3] G. Brida, M. Genovese, and I. Ruo Berchera, Nat. Photon. **4**, 227 (2010).
[4] E. D. Lopaeva, I. Ruo Berchera, I. P. Degiovanni, S. Olivares, G. Brida, and M. Genovese, Phys. Rev. Lett. **110**, 153603 (2013).
[5] G. Brida, I. P. Degiovanni, M. Genovese, M. L. Rastello, and I. Ruo Berchera, Opt. Express **18**, 20572 (2010).
[6] F. Hudelist, J. Kong, C. Liu, J. Jing, Z. Y. Ou, and W. Zhang, Nat. Commun. **5**, 3049 (2014).
[7] F. Khalili, S. Danilishin, H. Miao, H. Muller-Ebhardt, H. Yang, and Y. Chen, Phys. Rev. Lett. **105**, 070403 (2010).
[8] O. Jedrkiewicz *et al.*, Opt. Express **19**, 12903 (2011).
[9] While in low-gain PDC, correlated are only photon numbers of 0 and 1 and higher photon numbers occur with a very small probability, in high-gain PDC there is correlation between a larger set of photon numbers.
[10] R. S. Bennink and R. W. Boyd, Phys. Rev. A **66**, 053815 (2002).
[11] W. Wasilewski, A. I. Lvovsky, K. Banaszek, and C. Radzewicz, Phys. Rev. A **73**, 063819 (2006).
[12] Barak Dayan, Phys. Rev. A **76**, 043813 (2007).
[13] Andreas Christ, Benjamin Brecht, Wolfgang Mauerer, and Christine Silberhorn, New J. Phys. **15**, 053038 (2013).
[14] Andreas Eckstein, Benjamin Brecht, and Christine Silberhorn, Opt. Express **19**, 13770 (2011).
[15] M. V. Fedorov, M. A. Efremov, A. E. Kazakov, K. W. Chan, C. K. Law, and J. H. Eberly, Phys. Rev. A **69**, 052117 (2004).
[16] S. L. Braunstein, Phys. Rev. A **71**, 055801 (2005).
[17] E. Brambilla, A. Gatti, M. Bache, and L. A. Lugiato, Phys. Rev. A **69**, 023802 (2004).
[18] E. Brambilla, L. Caspani, O. Jedrkiewicz, L. A. Lugiato, and A. Gatti, Phys. Rev. A **77**, 053807 (2008).
[19] E. Brambilla, L. Caspani, L. A. Lugiato, and A. Gatti, Phys. Rev. A **82**, 013835 (2010).
[20] L. J. Wang, C. K. Hong, and S. R. Friberg, J. Opt. B **3**, 346 (2001).
[21] C. K. Law and J. H. Eberly, Phys. Rev. Lett. **92**, 127903 (2004).
[22] M. V. Fedorov, M. A. Efremov, P. A. Volkov, E. V. Moreva, S. S. Straupe, and S. P. Kulik, Phys. Rev. Lett. **99**, 063901 (2007).
[23] F. M. Miatto, H. di Lorenzo Pires, S. M. Barnett, and M. P. van Exter, Eur. Phys. J. D **66**, 263 (2012).
[24] F. M. Miatto, T. Brougham, and A. M. Yao, Eur. Phys. J. D **66**, 183 (2012).
[25] A. Perez, A. Cavanna, F. Just, M. V. Chekhova, and G. Leuchs, Laser Phys. Lett. **10**, 125201 (2013).
[26] A. Cavanna, A. M. Perez, F. Just, M. V. Chekhova, and G. Leuchs, Opt. Express **22**, 9984 (2014).
[27] K. Yu. Spasibko, T. Sh. Iskhakov, and M. V. Chekhova, Opt. Express **20**, 0507 (2012).
[28] T. Sh. Iskhakov, A. M. Pérez, K. Yu. Spasibko, M. V. Chekhova, and G. Leuchs, Opt. Lett. **37**, 1919 (2012).
[29] A. M. Pérez, T. Sh. Iskhakov, P. Sharapova, S. Lemieux, O. V. Tikhonova, M. V. Chekhova, and G. Leuchs, Opt. Lett. **39**, 2403 (2014).

[30] Alessia Allevi and Maria Bondani, J. Opt. Soc. Am. B **31**, B14 (2014).

[31] G. Brida, A. Meda, M. Genovese, E. Predazzi, and I. Ruo-Berchera, J. Mod. Opt. **56**, 201 (2009).

[32] A. Allevi, O. Jedrkiewicz, E. Brambilla, A. Gatti, J. Perina, Jr., O. Haderka, and M. Bondani, Phys. Rev. A **90**, 063812 (2014).

[33] L. J. Wang, X. Y. Zou, and L. Mandel, Phys. Rev. A **44**, 4614 (1991).

[34] P. Grangier, R. E. Slusher, B. Yurke, and A. LaPorta, Phys. Rev. Lett. **59**, 2153 (1987).

[35] D. N. Klyshko, Zh. Eksp. Teor. Fiz. **104**, 2676 (1993) [JETP **77**, 222 (1993)].